Multi-Omics Analysis Unveils Nsun5-Mediated Molecular Alterations in the Somatosensory Cortex and Its Impact on Pain Sensation

Authors

Peipei Chen, Heyu Zhao, Xia Gao, Junchao Xu, Zhili Huang, and Huali Shen

Correspondence

huangzl@fudan.edu.cn;
shenhuali@fudan.edu.cn

In Brief

Nsun5, a newly identified methyltransferase, plays a crucial role in cortical function. We provide evidence of the impact of Nsun5 on the structure of the primary somatosensory cortex. Using a multi-omics approach, we find that Nsun5 deletion affects translation, neurotransmitter metabolism, and synaptic transmission. Notably, Nsun5 deficiency reduces pain sensitivity. These findings highlight Nsun5's role in modulating S1 cortex thickness and pain perception, offering new insights into its broader functions in the brain and implications for neural health.

Graphical Abstract

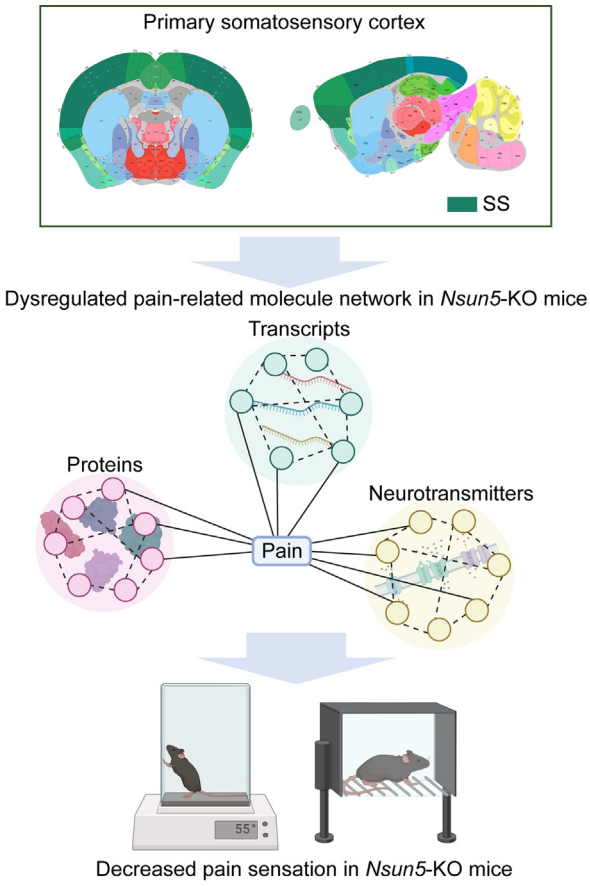

Highlights

- Transcriptome-proteome data identified Nsun5's role in S1 cortex functions.
- Loss of Nsun5 in the S1 cortex led to significant changes in neurotransmitter levels.
- Loss of Nsun5 reduced pain sensitivity and alterations in pain-related molecules.

2025, Mol Cell Proteomics *24*(*5*), 100960

https://doi.org/10.1016/j.mcpro.2025.100960

Multi-Omics Analysis Unveils Nsun5-Mediated Molecular Alterations in the Somatosensory Cortex and Its Impact on Pain Sensation

Peipei Chen[1,2,‡], Heyu Zhao[2,‡], Xia Gao[3], Junchao Xu[4], Zhili Huang[1,*], and Huali Shen[2,*]

Nsun5 assumes a pivotal role in the regulation of RNA methylation, and its deficiency has been linked to the advancement of hepatocellular carcinoma, gliomas, tetralogy of Fallot, cognitive deficits in Williams–Beuren syndrome, and brain development. This underscores Nsun5's significant involvement in the nervous system. In this study, we present evidence of Nsun5's influence on the structure of the primary somatosensory cortex. Through comprehensive multi-omics analyses, we unveil a spectrum of systematically altered genes and proteins, collectively engaged in the orchestration of translation, neurotransmitter metabolism, nerve conduction, synaptic transmission, and other functions. Notably, there are discernible changes in molecules associated with pain sensation, strongly indicating that Nsun5 deficiency undermines pain-related behavior. This study establishes a clear link between Nsun5 deficiency and transcriptional and proteomic changes, as well as neurotransmitter expression within the primary somatosensory cortex, and uncovers its novel role in impaired pain perception.

RNA modifications significantly affect the biogenesis and function of coding and noncoding RNAs, mediate metabolism, and play regulatory roles in disease initiation and progression. Currently, over 170 distinct RNA modifications have been identified (1). Among these, 5-methylcytosine stands out as the most abundant in tRNA and rRNA. m^5C methylation of RNA mainly catalyzed by members of the NOL1/NOP2/sun family and DNMT2, assumes paramount importance for RNA stability and functionality.

Nsun5 has emerged as a novel methyltransferase with multifaceted implications. It engenders methylation of RNAs, thereby influencing their stability, subcellular localization, and interactions with other molecular entities. Notably, the deficiency of mammalian Nsun5 yields diminished protein synthesis, which, in turn, impacts cell size and proliferation (2). This could be attributed to the maintenance of the tertiary rRNA-tRNA-mRNA complex due to m^5C3782 (3). In the cardiovascular system, Nsun5-mediated m^5C modification is indispensable for sustaining the expression of Tpm1, a gene pivotal for normal cardiac outflow tract morphogenesis, implicating Nsun5's involvement in tetralogy of Fallot (4). Additionally, Nsun5 exhibits pronounced upregulation in hepatocellular carcinoma and head and neck squamous cell carcinoma, correlating with poor prognosis predictions (5, 6). In glioma patients, epigenetic inactivation of NSUN5 correlates with tumor-suppressive attributes (3). Moreover, *NSUN5* is one of the heterozygous deletion genes in Williams-Beuren syndrome, previous work in our lab has initially discovered that Nsun5 is critical for cerebral cortex development (7), and Nsun5 deficiency leads to agenesis of the corpus callosum and dysfunction of the NMDA receptor in hippocampal pyramidal cells (8, 9), hinting at unexplored functions within the nervous system.

The primary somatosensory (S1) cortex is well-known for its role in processing sensory input from diverse body regions (10). Apart from its somatosensory processing functions, S1 also contributes to modulating tactile attention (11), integrating somatosensory and motor information (12), and influencing emotional responses (13). Moreover, S1 cortex receives both innocuous and noxious signals *via* thalamocortical inputs from the ventral posterolateral thalamus, and is, therefore, a primary junction at which body sensations can be amplified into pain or, conversely, painful signals can be attenuated (14). S1 cortex is responsible for somatic discriminating aspects of pain processing, such as location, intensity, and mass of pain (15, 16). Despite known contributions of S1 to sensory gain modulation, its exact role in somatosensation for pain remains a topic of debate. Given the notable expression of Nsun5 in the cortex, our investigation seeks to unravel its contribution to cortical functioning through a comprehensive "multi-omics" approach.

From the [1]Department of Pharmacology, School of Basic Medical Sciences, and [2]Department of Systems Biology for Medicine and Institutes of Biomedical Sciences, Shanghai Medical College, Fudan University, Shanghai, China; [3]Department of Experimental Surgery, Tangdu Hospital, The Fourth Military Medical University, Xi'an, Shanxi, China; [4]Department of Engineering, University of Pennsylvania, Philadelphia, USA
‡These authors contributed equally to this work.
*For correspondence: Zhili Huang, huangzl@fudan.edu.cn; Huali Shen, shenhuali@fudan.edu.cn.

https://doi.org/10.1016/j.mcpro.2025.100960

EXPERIMENTAL PROCEDURES

Experimental Design and Statistical Rationale

We applied the Nissl staining on the brain sections to observe the morphology of the cerebral cortex in the three-month-old littermates of WT and *Nsun5*-KO mice. To further investigate the Nsun5-induced molecular variations, according to the mouse brain atlas, the S1 cortex tissues from Bregma –0.11 mm to –0.83 mm anatomical locations were isolated, and then the transcriptome, proteome, and targeted metabolomics were profiled. In above omics analysis, four, five, and four biological replicates were applied for each group of samples, respectively (Fig. 1*B*). The "omics" data were subjected to bioinformatics analysis, including difference identification, Gene Ontology (GO) functional enrichment, pathway enrichment, and integrative multi-omics analysis (Fig. 1*C*), and so on. Finally, based on the analysis and insights derived from multiple omics studies, we selected pain-related molecules for validation at the gene and protein levels. Additionally, we assessed nociceptive behavior through hot plate and Von Frey assays in seven biological replicates. Data were expressed as mean ± standard error (mean ± SEM), statistical analysis was performed using SPSS19.0 software, and Prism 9.0 software was used for graphing. Student's *t* test and post hoc multiple comparison analysis of variance (ANOVA) were used for statistical analysis, and $p < 0.05$ was considered statistically significant.

Generation and Identification of Nsun5 Null Mice

The procedures involving animals and their care were conducted in accordance with the ARRIVE guidelines of Laboratory Animal Care. All animal experiments were approved by the Institutional Animal Care and Ethical Committee of Fudan University (No. 201909005S) and were performed following the guidelines of the Laboratory Animal Research Institute for Experimental Animals of Fudan University. All efforts were made to minimize animal suffering and to reduce the number of animals used. The mice were maintained under constant environmental conditions (temperature of 23 ± 2 °C, humidity of 55 ± 5%, and a 12: 12-h light/dark cycle) in the Animal Research Center of Fudan University with free access to food and water. The *Nsun5*-KO mouse was generated as previously described (17). The genotype was determined by PCR using the genomic DNA obtained from tail biopsies. The genotyping primers were as follows: 5′-CTGTCCAGGTGCTAGTGTATG-3′ and 5′-GGTCCTCATTTCGGCTCAC-3′. The size of the Nsun5 deletion was determined by the amplification of a 153 bp and/or 131 bp fragment.

Hot Plate

The mice were first placed in an experimental environment for 30 to 60 min of adaptation. The experiment was carried out on a self-made hot-plate device with the temperature of the hot-plate set at 55 ± 0.5 °C. The test was performed by gently placing the mice on a hot plate and immediately starting the timer. Observing and recording when the animal began to experience a painful reaction, such as licking or withdrawing the paw. If the animal did not react within 30 s, the animal was removed from the hot plate and the latency was recorded as 30 s (18).

Von Frey

The mice were first acclimated in the test cage for 30 to 60 min. Tests were conducted using Von Frey monofilms (0.008–300 g, Aesthesio, Danmic). Start by selecting a minimum filament from the left hind limb as the starting weight. Applying the fibers to the plantar surface of the back paw, exerting enough force on the fibers to bend and maintaining contact for 1 to 2 s. If the mice did not have a foot retraction reflex, the test was continued with the next heavier filament. There should be at least 2 min between tests. Continuously test the fiber and record as the result of the test the weight that triggers the foot retraction in 2 out of 3 tests. The test was then repeated on the right hind limb. Each limb was tested twice, with the animal tested in a left-right-left-right order (18).

Brain Tissue Preparation

Subsequently, 3-month-old male *Nsun5*-KO mice and WT littermates were selected and anesthetized with 2% pentobarbital sodium (45 mg/kg). To obtain individual S1 cortex samples for each brain, we combined the bilateral S1 cortices using a Neuro Punch (19). Brain tissues were taken out on ice, and frozen with liquid nitrogen.

Nissl Staining

Brain tissue was fixed with 4% paraformaldehyde for 6 to 8 h. The brain specimens were fixed, dehydrated, embedded, and sectioned. Then brain tissue sections were immersed in Nissl stain (C0117, Beyotime Biotechnology) for 30 min. Histological images were attained using a digital slide scanning system (Olympus VS200) and processed with software (Image-Pro Plus software 6.0) (20).

RNA Extraction and Detection

Total RNAs of tissue samples were extracted by Trizol, and the RNA samples were subjected to strict quality control through Agilent 2100 bioanalyzer to accurately detect the integrity of RNA before building the database.

Library Construction and Quality Inspection

The qualified total RNA was enriched with Oligo (dt) magnetic beads to get mRNA with poly A tail, and then shuffling mRNA enriched with bivalent cations. Using mRNA fragments as templates and random oligonucleotides as primers, we synthesized the first complementary DNA (cDNA) strand in the reverse transcriptase M-MuLV system and then used RNAase H enzyme to degrade excess RNA in the system. Using dNTPs as raw materials, in the DNA polymerase I system, the second cDNA chain was synthesized. The purified cDNA needed to undergo terminal repair, add A tail, and add joint, and then AMPure XP magnetic beads were used to screen the 370 to 420 bp cDNA for PCR amplification. After the amplification, AMPure XP magnetic beads were used to purify the PCR products. In the process of quality control, the library was quantified by Qubit 2.0 fluorometer and diluted to 1 to 2 ng/μl, and then the size of the inserted fragment of the library was detected by Agilent 2100 bioanalyzer. Then quantitative reverse transcription polymerase chain reaction (qRT-PCR) was used to accurately quantify the effective concentration of the library. After the library was checked correctly, paired-end 150 nt, Illumina sequencer was used to sequence the library, and the original data of each sample was 6 GB. The database construction and sequencing were completed by Novogene Co, Ltd.

RNA Sequence and Data Analysis

In order to ensure the reliability of subsequent data analysis, the data should be filtered to remove reads with joints, reads with unknown bases and low-quality reads, and the contents of Q20, Q30, and GC should be calculated in the clean data. Subsequent analyses were performed using clean data. HISAT2 algorithm V2.0.5 was used to construct the index of the reference genome and perform data comparison. Feature Counts algorithm was used to calculate the counts mapped to each gene. We calculated the fragments read per thousand base transcripts per million maps of each gene based on gene length. Using 1.20.0 DESeq2 algorithm for grouping KO and WT after the variance analysis, selection of meet the conditions of $p < 0.05$, $| \log_2 FC | > 0.58$ gene for the differences.

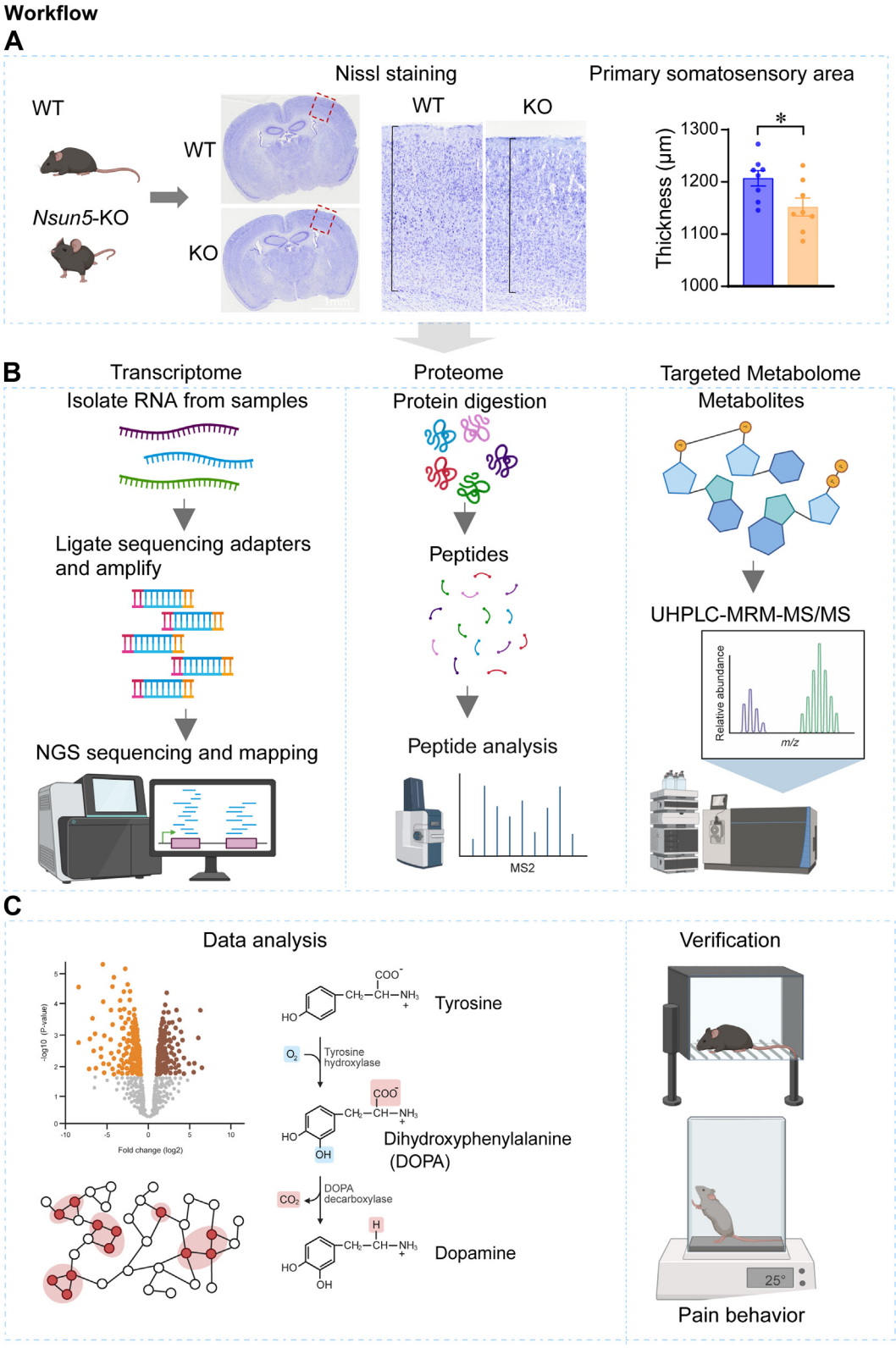

FIG. 1. **Workflow design of multi-omics analysis in S1 cortex**. *A*, Nissl staining illustrates cortical thickness comparisons between *Nsun5*-KO mice and wild-type (WT) littermates. *B*, detailed workflow diagram displaying the process of isolating and analyzing brain tissue from specific regions of the S1 cortex. N = 8 biological replicates for WT and KO group, respectively. Two-tailed independent *t* test. Data are presented as mean ± SEM. Statistical significance is noted as $^{*}p < 0.05$ and $^{**}p < 0.01$. *C*, schematic representation of the methods used for RNA sequencing, proteome analysis, and targeted metabolomics, leading to downstream data analysis and verification involving differential expression studies and assessments of pain behavior in *Nsun5*-KO mice compared to WT.

Gene Ontology and Kyoto Encyclopedia of Genes and Genomes Analysis

The Gene Ontology resource (http://geneontology.org) and Metascape resource (http://metascape.org/gp/index.html#/main/step1) were used to perform bioinformatics analyses including GO and Kyoto Encyclopedia of Genes and Genomes (KEGG) pathway enrichment. GO term and KEGG term with $p < 0.05$ were considered enriched for differential genes.

Sample Preparation

Five volumes of lysate (2% SDS + 20 mM Hepes) were added to the brain tissue sample, followed by centrifugation at 14,000 rpm for 15 min. The supernatant was then aspirated. Protein concentration was determined using a BCA assay kit (Product #23227, Thermo Fisher Scientific). To 200 μg of protein, 10 mM DTT was added, incubated at 56 °C for 30 min, followed by the addition of 20 mM iodoacetamide and further incubation for 30 min at 37 °C at 850 rpm. Subsequently, five volumes of acetone were added to the sample and incubated at –20 °C overnight. The mixture was centrifuged at 4 °C for 10 min, the supernatant was discarded, and the pellet was washed with 500 μl acetone. After a second centrifugation, the supernatant was discarded, and the pellet was air-dried in a fume hood. The protein was redissolved in NH_4HCO_3 to a final concentration of 1 μg/μl. LysC was added at a mass ratio of 1:100, and the mixture was incubated for 6 h; trypsin was then added and the mixture was incubated overnight at 37 °C. The enzymatic reaction was terminated by adding TFA to a final concentration of 0.8%, 30 min after the last addition. A 50 mg C18 filler column was prepared, initially activated with two 200 μl aliquots of 100% acetonitrile (ACN), and then equilibrated with two 600 μl aliquots of 0.1% TFA. The sample was applied to the column slowly, washed twice with 200 μl of 0.1% TFA, and eluted using a gradient of 100 μl each of 50% ACN +0.1% TFA and 80% ACN +0.1% TFA. The eluate was lyophilized using a vacuum freeze concentrator and stored at –20 °C. Chromatographic separation was performed on a nanoElute (Bruker Daltonics) using a 250 mm × 75 μm column (IonOpticks). Mobile phases A and B consisted of water and ACN, respectively, both containing 0.1% formic acid (FA). The flow rate was set at 300 nl/min, with a total analysis time of 1 h. The gradient of phase B was increased from 2% to 22% over 45 min, ramped up to 37% in the next 5 min, then to 80% in another 5 min, and held there for an additional 5 min. A total of 200 ng of peptides were used for subsequent LC-MS analysis.

High-pH Reversed-phase Fraction

The peptide mixture obtained after preprocessing of whole-brain tissue was reconstituted in buffer A (20 mM ammonium formate aqueous solution, pH 10.0). Subsequently, it was subjected to high-pH separation using the Ultimate 3000 system connected to a reverse-phase column (XBridge C18 column, 4.6 mm × 250 mm, 5 μm, Waters Corporation). The separation employed a linear gradient over a total duration of 40 min, ranging from 5% to 45% of solvent B (80% ACN with the addition of 20 mM ammonium formate, pH 10.0). The column was equilibrated for 15 min, with a flow rate maintained at 1 ml/min and a column temperature of 30 °C. A total of 20 fractions were collected and dried using a vacuum concentrator.

The desalted and lyophilized peptide segments were then reconstituted in a 0.1% FA aqueous solution and subjected to liquid chromatograph-mass spectrometer/mass spectrometer (LC-MS/MS) analysis. The entire system consisted of the tandem UltiMate 3000 system coupled with the trapped ion mobility spectrometry and time-of-flight mass spectrometry Pro mass spectrometer. A total of 200 ng of sample was injected (column: 25 cm × 75 μm i.d., IonOpticks), and separation was carried out over 60 min with a column temperature of 50 °C. Each sample was injected in a volume of 2 μl, and the column flow rate was controlled at 300 nl/min. The gradient started at 4% of solvent B and increased to 28% within 45 min, then further increased to 44% in 10 min, followed by a 7-min gradient to 90%, which was maintained for 8 min.

Database Construction Using Nano-ultra-high performance liquid chromatography-tandem mass spectrometry (UHPLC-MS/MS) Based on DDA

The mass spectrometer was operated in data-dependent acquisition (DDA) PASEF mode with the following parameter settings: 10 PASEF scans were performed in each cycle, with an accumulation time of 100 milliseconds per scan; scan range spanned from 100 to 1700 m/z (mass-to-charge ratio); ion mobility (1/K0) range was set from 0.6 to 1.6; scan charge state ranged from 0 to 5; target value is set at 10,000; dynamic exclusion was applied for 0.4 min. The isolation window width was set to 2 Th (Thomson) when m/z was less than 700 and 3 Th when m/z was greater than 700.

The raw data collected through DDA were merged and analyzed using Peaks Online software version 1.7 (Bioinformatics Solutions Inc) for database searching. The database used was the mouse database downloaded from SwissProt (comprising 17,046 proteins, downloaded on August 20, 2020). Trypsin digestion was set as the enzyme cleavage rule. In the search parameters, the fixed modification was set to carbamidomethyl, and the variable modification was set to methionine oxidation. The mass tolerance for precursor ions was set to 20.00 PPM, and for fragment ions, it was set to 0.05 Da. We allowed up to 2 missed cleavages during the search. The false discovery rate (FDR) at the peptide level was set to 1%, and the FDR at the protein level was also set to 1%.

DIA-PASEF Processing

The trapped ion mobility spectrometry and time-of-flight mass spectrometry Pro mass spectrometer (Bruker Daltonics) was used to analyze the peptide segment. For the dia-PASEF measurements, survey full-scan mass spectra were acquired across the mass range of 100 to 1700 m/z in positive electrospray mode. One MS1 full scan was followed by 27 dia-PASEF scans with variable widths. The method covers an m/z range from 300 to 1200 with two IM windows per dia-PASEF scan ranging from 0.75 to 1.37 Vs/cm^2. The ion source voltage was maintained at 1500 V, the auxiliary gas flow rate was set at 3 L/min, and the ion source temperature was held at 180 °C. The raw data obtained from the DIA were imported into Peaks Online software using default settings. The mass tolerance for precursor ions was set to 20.00 PPM, and for fragment ions, it was set to 0.05 Da. The FDR for both peptide spectrum matches and protein groups was controlled at 1%. A decoy database was generated using a mutated strategy. Quantification in PEAKS was performed using the label-free quantification algorithm.

Targeted Metabolomics for Neurotransmitter Measurement

Neurotransmitters were extracted and measured using the targeted metabolomics method with modifications. An aliquot of each individual sample was precisely weighed and transferred to an Eppendorf tube. After the addition of 80 μl of extract solvent (precooled at - 20 °C, ACN, within 0.1% FA) and 20 μl of H_2O, the samples were vortexed for 30 s, homogenized at 45 Hz for 4 min, and sonicated for 5 min in an ice-water bath. The homogenate and sonicate circle were repeated three times, followed by subsiding at - 40 °C overnight and centrifuging at 12,000 rpm and 4 °C for 15 min. And 80 μl of the supernatants were transferred to the EP tube, and incubated for 30 min after adding 40 μl 100 mmol/L sodium carbonate solution and 40 μl 2% benzoyl chloride ACN solution. The samples were centrifuged at

12,000 rpm for 15 min at 4 °C after the addition of 10 μl internal standard. The 40 μl of the supernatants were added in 20 μl H_2O and then transferred to an autosampler vial for UHPLC-MS/MS analysis. The UHPLC separation was carried out using an ExionLC System, equipped with a Waters ACQUITY UPLC HSS T3 (100 × 2.1 mm, 1.8 μm). The mobile phase A was 0.1% FA and 1 mM/L ammonium acetate in water, and the mobile phase B was ACN. The column temperature was set at 40 °C. The autosampler temperature was set at 4 °C, and the injection volume was 1 μl. AB Sciex QTrap 6500+ mass spectrometer was applied for assay development. Typical ion source parameters were as follows: IonSpray Voltage: +5000V, Curtain Gas: 35 psi, Temperature: 400 °C, Ion Source Gas 1: 60 psi, Ion Source Gas 2: 60 psi. Skyline Software was employed for multiple reaction monitoring data processing. The final concentration (CF, nmol/L) equals the calculated concentration (Cc, nmol/L) multiplied by the dilution factor (Dil). The metabolite concentration (CM, nmol/g) equals the final concentration multiplied by the final volume (VF, mL), and divided by the weight (Ms, mg) of the sample.

Real-Time Quantitative Polymerase Chain Reaction (RT-PCR)

RNAseq data were validated by RT-PCR on mRNA extracted from the S1 cortex of WT and KO mice. All primer sequences were selected from previous literature on mouse brain tissue or designed using Primer3 (http://bioinfo.ut.ee/primer3/). Confirm primer specificity for the target sequence using NCBI Primer-BLAST (https://www.ncbi.nlm.nih.gov/tools/primer-blast/) and test primer-dimers using a DNA gel to demonstrate its PCR The product produced a band of the expected size. Finally, denaturation curves performed after RT-PCR cycles with intercalating dyes were analyzed to ensure that there was a distinct peak in the negative derivative of fluorescence *versus* temperature. This indicates that the amplified dsDNA product is not due to nonspecific amplification. Transcripts enriched in the S1 cortex at baseline were normalized to GAPDH levels for each sample (all primer sequences listed in Extended Data).

Western Blot

Whole protein extraction was the same as the proteomics tissue pretreatment method mentioned above. The extracted protein supernatant was stored in aliquots at – 80 °C. Equal amounts of proteins were separated by SDS-PAGE and transferred to the polyvinylidene fluoride membrane. Membranes were blocked with 5% skim milk containing Tris-buffered saline/Tween-20 and then incubated with antibodies against rabbit anti-Ache (1:1000, ab97299, Abcam), or rabbit anti-Rtn4r (1:10,000, ab184556, Abcam) at 4 °C for 24 h. The horseradish peroxidase-conjugated secondary antibody was incubated with the membrane for 1 h at room temperature, and the signal was visualized using an enhanced chemiluminescence detection kit. The Western blot bands were scanned and analyzed using the ImageJ software.

RESULTS

Nsun5 Deficiency Induced Changes in the Thickness of Multiple Cortical Regions

In *Nsun5*-KO mice, we detected significant reductions in cortical thickness within multiple cortical regions. Quantitative analysis revealed that the visual, retrosplenial, somatomotor, and S1 cortices were notably thinner in *Nsun5*-KO mice compared to WT controls (Fig. 1*A* and supplemental Fig. S5), while no differences were observed in the auditory cortex, PTLp, or visceral cortex. *In situ* hybridization data from the Allen Mouse Brain Atlas indicated that Nsun5 expression is markedly elevated in both the motor and S1 cortices relative to other cortical areas (https://mouse.brain-map.org/gene/show/64779). Notably, the reduction in thickness was more pronounced in the S1 cortex than in the somatomotor cortex, prompting us to focus subsequent analyses on the S1 region.

Nsun5 Deficiency Induced Transcriptomic Alterations in the S1 Cortex

To assess whether Nsun5 deficiency alters the transcriptome and proteome of the S1 cortex, we performed next-generation RNA-sequencing (RNA-seq) and DIA proteome on S1 cortex tissues of WT and *Nsun5*-KO mice. For the transcriptome, we sequenced four biological replicates per group to obtain high statistical power. Paired-end 150 nt, Illumina sequencer was used to sequence the library, and the original data size of each sample was more than 6 GB. There were 12,423 and 12,417 genes identified in WT and KO mice and 12,415 genes were found expressed in both groups (supplemental Fig. S1*A*). A principal component analysis was used to visualize variations and to highlight robust patterns of the WT and *Nsun5*-KO datasets in a two-dimensional score plot. The first principal component indicated a clear separation between the KO and WT littermates (Fig. 2*A*). Differentially expressed genes were defined based on a fold-change>1.5, $p < 0.05$ when comparing *Nsun5*-KO to WT mice. The volcano plot illustrated 166 upregulated and 256 downregulated transcripts, respectively (Fig. 2*B*). Furthermore, a distinct pattern in gene expression profiles between WT and KO mice emerged from hierarchical clustering. Notably, the most drastically downregulated genes such as period circadian protein homolog 2 (Per2) (21), Xanthine dehydrogenase/oxidase (Xdh) (22), Aromatic-L-amino-acid decarboxylase (Ddc) (23), dimethylaniline monooxygenase [N-oxide-forming] 2 (Fmo2) and Klf2 (24), as well as the upregulated genes such as Gabrb2 (25) and Arg2 (26), have been previously linked to pain sensitivity (Fig. 2*C*). Additionally, GO analysis disclosed that those downregulated genes primarily participate in vital biological processes such as translation and cellular metabolism (oxidative phosphorylation, generation of precursor metabolites, and energy), analyzes also revealed changes in rhythmic function and ribosomal subunit composition, suggesting that Nsun5 deficiency interrupted ribosome components and cellular metabolism processes (Fig. 2*D*). While the upregulated transcripts participated in processes of nerve conduction and synaptic transmission (axonogenesis, regulation of membrane potential, ion transport, ion channel activity, and neuron-to-neuron synapse) (Fig. 2*D*). Furthermore, Nsun5 was found to be a positive regulator of nicotine addiction, morphine addiction, and GABAergic pathways through a KEGG pathway enrichment. Besides, Nsun5 exerts a negative regulatory influence on genes associated with ribosomes, oxidative phosphorylation, thermogenesis, and circadian rhythm (Fig. 2*E*). To validate the observed gene expression disparities in the RNA-Seq dataset, a quantitative PCR analysis of select

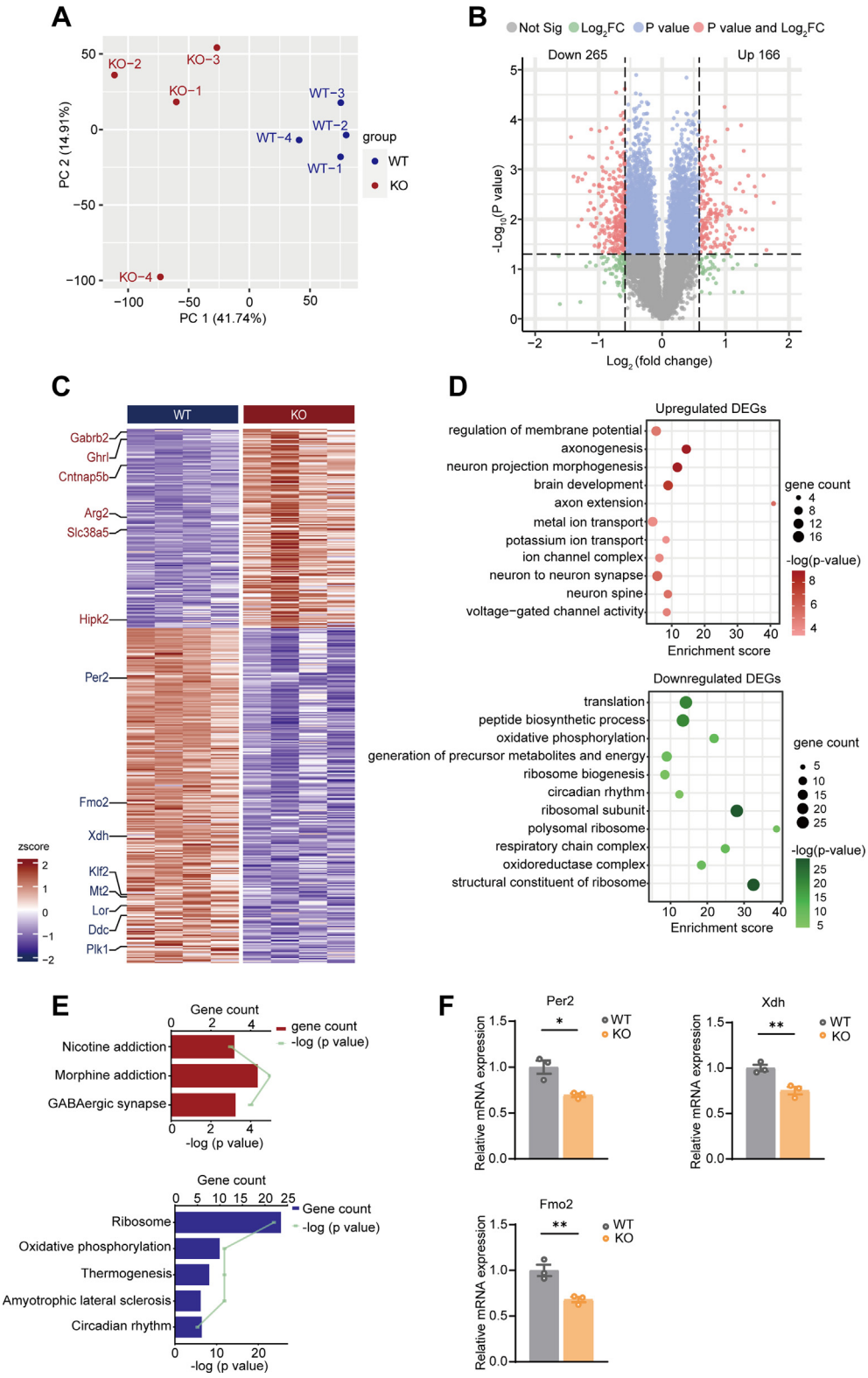

FIG. 2. **Transcriptomic changes induced by Nsun5 deficiency in the S1 cortex.** *A*, PCA illustrating distinct clustering within the WT and *Nsun5*-KO groups and clear separation between the two groups. *B*, volcano plot highlighting differential gene expression in the S1 cortex. Genes significantly changed are marked in *red*. The *horizontal line* indicates $p < 0.05$, and the *vertical lines* represent a log2 fold change greater than ±0.58. *C*, heatmap displaying differential expression of genes between WT and *Nsun5*-KO mice, with data normalized to z-scores. *D*, GO analysis of upregulated and downregulated DEGs revealing enriched biological processes. The size of each circle corresponds to the number of

genes—Per2, Fmo2, and Xdh, known to modulate pain sensation—was conducted. This analysis demonstrated a higher level of mRNA expression consistency when compared to the RNA-Seq dataset (Fig. 2*F*). Overall, the absence of Nsun5 induced changes in transcripts within the S1 cortex, prominently affecting gene expression dysregulation. The differential genes were notably engaged in critical biological processes, including cell metabolism, ribosome components, nerve conduction, and synaptic transmission.

Nsun5 Deficiency Induced Proteomic Alterations in the S1 Cortex

In DIA data analysis, the mouse-brain-specific DDA library was built based on peptide identifications from a separate DDA experiment. Raw DIA data of S1 tissues were then processed for peptide identification and quantification using a peptide-centric scoring algorithm against this experimental DDA library. As a result, we identified 6310 and 6330 proteins in the S1 cortex of *Nsun5*-KO and WT mice (supplemental Fig. S2*A*) respectively, of which 566 proteins were significantly regulated in *Nsun5*-KO mice ($p < 0.05$, fold-change >1.5) compared with WT. Principal component analysis visualized variations and robust patterns in the datasets in a two-dimensional score plot of WT and *Nsun5*-KO mice (Fig. 3*A*). The volcano plot showed that 293 proteins were upregulated while 273 proteins were downregulated in the KO *versus* WT group (Fig. 3*B*). Hierarchical clustering divided these proteins into two clusters. The top differential proteins include Rac3 (27), Itsn1 (28), Igf2bp3, Glb1, Entpd2, Impa2 (29), Eif2b1 (30), Rtn4r, and acetylcholinesterase (Ache) which were known to be associated with neuronal activity, cortex structure, and pain sensation (Fig. 3*C*). In detail, the downregulated proteins are enriched in biological processes such as translation, rRNA binding processes, axon development, and ion channel regulator activity. Additionally, significant cellular components associated with these downregulated proteins include ribosomal subunits and neuron-to-neuron synapses. On the contrary, the upregulated proteins play a distinct role in oxidative phosphorylation, neurotransmitter transport, and synaptic vesicle dynamics (Fig. 3*D*). We used the KEGG database to reveal those dysregulated pathways. The outcomes showed that up-regulated proteins affected metabolic and apoptotic pathways such as oxidative phosphorylation, thermogenesis, and cellular senescence, while downregulated proteins affected the ribosome and endocytosis pathways (Fig. 3*E*). To further substantiate our findings, we conducted Western blot analyses on two representative proteins, Rtn4r and Ache, within the S1 cortex of both WT and *Nsun5*-KO mice, as depicted in Figure 3*F*. These experiments not only validated the outcomes of our quantitative proteomic analysis but also showcased how Nsun5 deficiency induces alterations in protein expression levels within the S1 cortex. These alterations notably impact the regulation of translation, cell metabolism, neuron development, nerve conduction, and synaptic transmission.

Correlation Analysis of the Proteomic and Transcriptomic Data in S1 Cortex

To better characterize the transcriptional and proteomic dynamic in mice loss of Nsun5, we next performed a combined analysis with the omics data in *Nsun5*-KO and WT mice. A total of 5461 out of 11,388 protein-coding transcripts were detected at the protein level, representing deep coverage of the proteomic dataset (Fig. 4*A*). A scatter plot of association analysis by log2-fold change at transcript and protein level was subdivided into four quadrants, that showed increase/decrease in protein (red) or mRNA (blue) only or both (purple). The 51 and 73 transcripts/proteins in the quadrant 1 and 3 showed consistent expressional trends. The 40 and 83 transcripts/proteins in quadrants 2 and 4 showed negative expressional trends (Fig. 4*B*). These molecules showed significant expression changes at both the transcript and protein levels, indicating high consistency in gene expression regulation. GO analysis was performed to compare the gene function in terms of their similarities and differences comparing *Nsun5*-KO and WT mice. Enrichment analysis of consistently upregulated mRNAs and proteins indicated predominant enrichment in synaptic transmission, synaptic structure, and ERBB4 signaling pathways. Consistently downregulated mRNAs and proteins were primarily associated with biological processes including regulation of translation, ribosome biogenesis, and cell volume homeostasis (Fig. 4*D*). Additionally, heatmaps were used to visualize the specific differential molecules associated with the GDP binding, postsynaptic membrane, ribosomal subunit, and ribonucleoprotein complex binding processes (Fig. 4*F*). Moreover, we observed that the majority of molecules associated with pain perception, including Gnai1, Kras, Slc6a1, and Cntn1, displayed consistent trends between mRNA and protein expression levels. Only 5 molecules showed consistent and significant differences in transcription and protein levels comparing *Nsun5*-KO to WT mice (fold-change>1.5, $p < 0.05$) (Fig. 4*C*). Molecules that were downregulated at the mRNA level but upregulated at the protein level predominantly enriched in processes such as GTPase complex, regulation of

genes involved, and the color indicates the level of statistical significance. *E*, KEGG pathway analysis of the DEGs in the S1 cortex, showing top significantly enriched pathways. *F*, bar graphs presenting relative mRNA expression levels of Per2, Fmo2, and Xdh as analyzed by RT-PCR in *Nsun5*-KO compared to WT mice. N = 3 biological replicates for WT and KO group, respectively. Two-tailed independent *t* test. Error bars indicate ±SEM. Statistical significance is noted as $^{*}p < 0.05$ and $^{**}p < 0.01$. KEGG, Kyoto Encyclopedia of Genes and Genomes; RT-PCR, real-time quantitative PCR; PCA, principal component analysis; Xdh, xanthine dehydrogenase/oxidase; GO, Gene Ontology; DEG, differentially expressed gene.

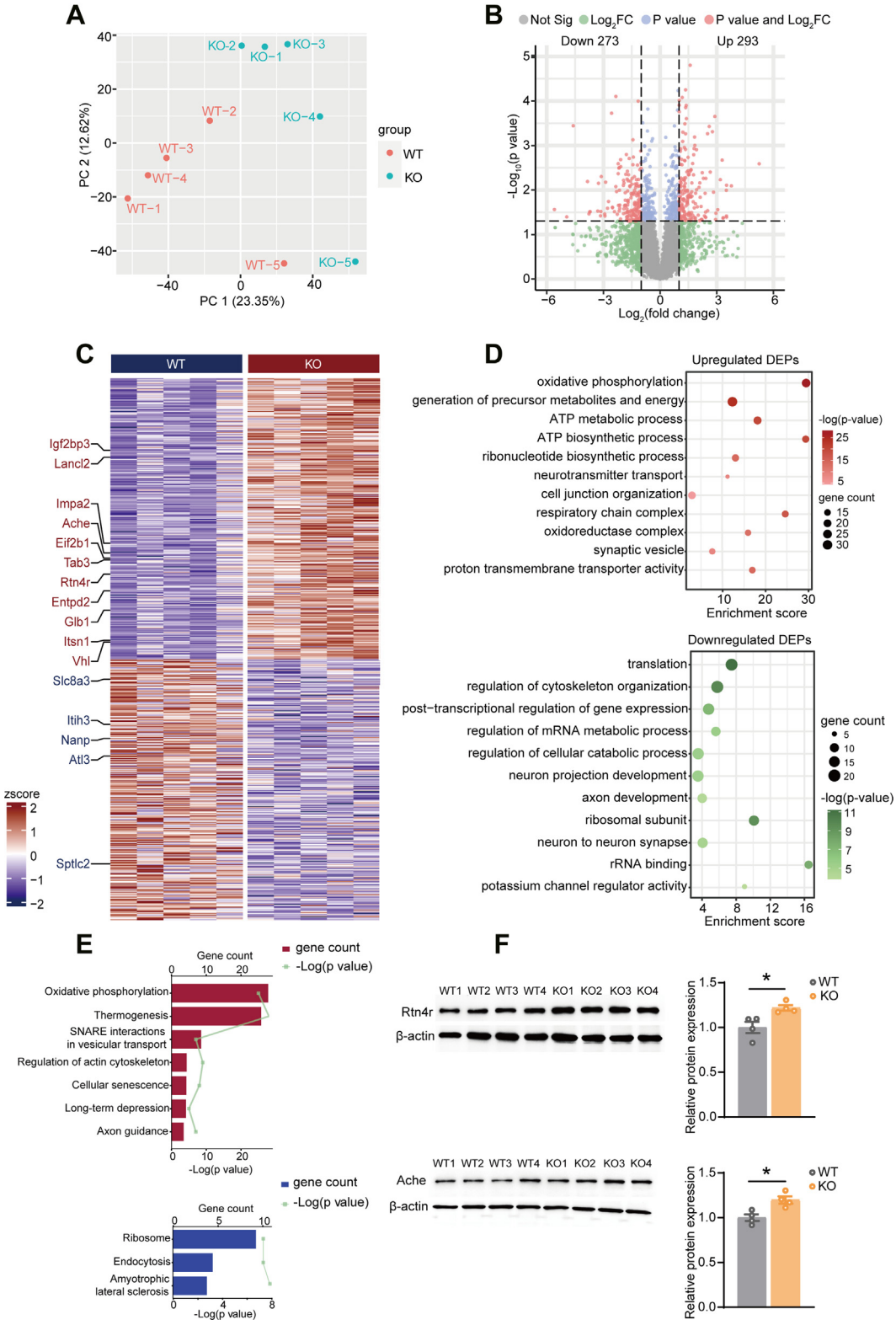

FIG. 3. **Proteomic analysis in the S1 cortex of *Nsun5*-KO *versus* WT mice.** *A*, PCA demonstrating distinct clustering between WT and *Nsun5*-KO mouse groups, based on proteomic profiles. *B*, volcano plots illustrating the differential protein expression between WT and *Nsun5*-KO mice. The *horizontal line* indicates $p < 0.05$, and the *vertical lines* represent a log2 fold change greater than ±0.58. *C*, heatmap showed differential proteins between WT and *Nsun5*-KO mice, normalized to z-scores. *D*, GO analysis (selected most statistically significant processes in interests) of the upregulated and downregulated proteins in S1 cortex. *E*, KEGG pathway analysis of the up- and down-regulated proteins. *F*,

apoptosis, and oxidative phosphorylation. Conversely, molecules that were upregulated at the mRNA level but downregulated at the protein level mainly regulated the protein polymerization, neuron development, and cytoskeleton organization (Fig. 4*E*). Additionally, heatmaps highlighted specific differential molecules implicated in critical biological processes, including oxidative phosphorylation, myelin sheath formation, regulation of protein polymerization, and cytoskeletal organization (Fig. 4*G*). The negative correlation between mRNA and protein expression levels indicates the presence of complex regulatory mechanisms, potentially involving differences in mRNA stability, translation efficiency, protein degradation, and posttranslational modifications. NSUN5 deficiency altered the fidelity of mRNA translation and protein synthesis (2).

Neurotransmitters Were Significantly Altered in S1 Cortex in Nsun5*-KO Mice*

Through a combined analysis of transcriptome and proteome data, we have observed that Nsun5 deficiency leads to coordinated dysregulation of both transcripts and proteins involving cellular metabolism, translation, neuro-transduction, synaptic transmission, and so on, within the S1 cortex. These molecules are closely related to neurotransmitter expression. We then conducted a targeted metabolomics study (supplemental Fig. S4*A*) to assess the levels of 42 neurotransmitters within the S1 cortex. Out of these, 12 neurotransmitters exhibited statistically significant differences ($p < 0.05$, fold-change >1.5) and were categorized into four pathways: dopamine (DA), serotonin, serine (Ser), and acetylcholine (ACh). In the DA metabolic pathway, tyrosine and 3, 4-dihydroxyphenylalanine (DOPA) serve as the two precursors for DA biosynthesis, while 3, 4-dihydroxyphenylacetic acid (DOPAC) and homovanillic acid are the primary metabolites of DA (31, 32). In our study, reduced concentrations of DOPAC, tyrosine, and octopamine suggested a significant impact on the DA metabolic pathway due to Nsun5 deficiency (Fig. 5, *B* and *F*). Serotonin, on the other hand, is derived from tryptophan and 5-hydroxytryptophan (5-HTP), with 5-hydroxyindoleacetic acid (5-HIAA) being its metabolite (33). Notably, the concentration of 5-HIAA was markedly decreased in *Nsun5*-KO mice (Fig. 5, *B* and *E*). Similarly, within the ACh, serine, and glycine (Gly) biosynthesis pathways, we observed reduced concentrations of Gly, Ser, and L-Cysteine (Cys), coupled with an increase in ACh levels in KO mice (Fig. 5, *C* and *D*). Furthermore, the levels of other amino acid neurotransmitters, including L-Arginine (Arg), Putrescine (Put), L-Asparagine (Asn), and L-Lysine (Lys), were also found to be diminished in *Nsun5*-KO mice (Fig. 5*A*). Collectively, these findings indicated that Nsun5 deficiency profoundly affected neurotransmitter metabolism, nerve conduction, and synaptic transmission in the S1 cortex.

Nsun5 Deficiency Impaired the Pain Sensation

Our transcriptomic and proteomic analyses revealed alterations in several molecules known to play roles in the regulation of pain sensation, such as Xdh (34), Per2 (21), NOGO receptor 1 (Rtn4r/NgR1) (35), and Ache (36). Additionally, targeted metabolomics profiling of 42 neurotransmitters demonstrated significant changes in key modulators of pain perception, such as ACh, Gly, and DOPAC. In Figure 6*A*, we presented a molecular network comprising 5 genes, 54 proteins, and 5 neurotransmitters that collectively regulated pain perception and were influenced by Nsun5 deficiency. To further investigate the impact of Nsun5 deletion on pain sensation in mice, we conducted experiments using the hot plate test and Von Frey hair filaments as stimuli to assess nociception. The hot plate test, a widely recognized method for evaluating nociception in mice, involves placing a rodent on a heated surface within an enclosure and measuring the latency to lick a hind paw or jump out of the enclosure (37). Von Frey hair filaments are frequently used stimuli to measure mechanical nociception in rodents (38). The detection paradigm was shown in the Figure 6, *B* and *E*. The results showed KO mice displayed an increased tendency of escape latency ($p > 0.05$, Fig. 6, *C* and *D*) in the hot plate test and significantly increased mechanical threshold for paw withdrawal by Von Frey test ($p < 0.05$, Fig. 6, *F* and *G*), which indicated reduced pain sensitivity. In summary, the observed changes in the expression of molecules involved in cell metabolism and neurotransmission within the S1 cortex, resulting from Nsun5 deletion, were strongly associated with the diminished pain perception observed in *Nsun5*-KO mice.

DISCUSSION

In this study, we examined the effects of Nsun5 deletion on the morphology, molecular composition, and functionality of the S1 cortex. Our findings revealed that Nsun5 deficiency resulting in reduced cortical thickness of the S1 cortex.

Nsun5 has been reported to play crucial roles in cortical development (7). According to the Allen Mouse Brain Atlas *in situ* hybridization data, Nsun5 is highly expressed in both the somatosensory (S1) and motor cortices (https://mouse.brain-map.org/gene/show/64779). Here, we show that Nsun5 deficiency reduces the thickness of the visual, retrosplenial, S1,

Western blot analysis comparing the expression levels of Rtn4r and Ache proteins between WT and *Nsun5*-KO mice, with quantitative bar graphs showing relative protein expression normalized to β-actin. N = 4 biological replicates for WT and KO group, respectively. Two-tailed independent *t* test. Error bars represent ±SEM, with $^*p < 0.05$ indicating statistical significance. GO, Gene Ontology; KEGG, Kyoto Encyclopedia of Genes and Genomes; PCA, principal component analysis; Ache, acetylcholinesterase.

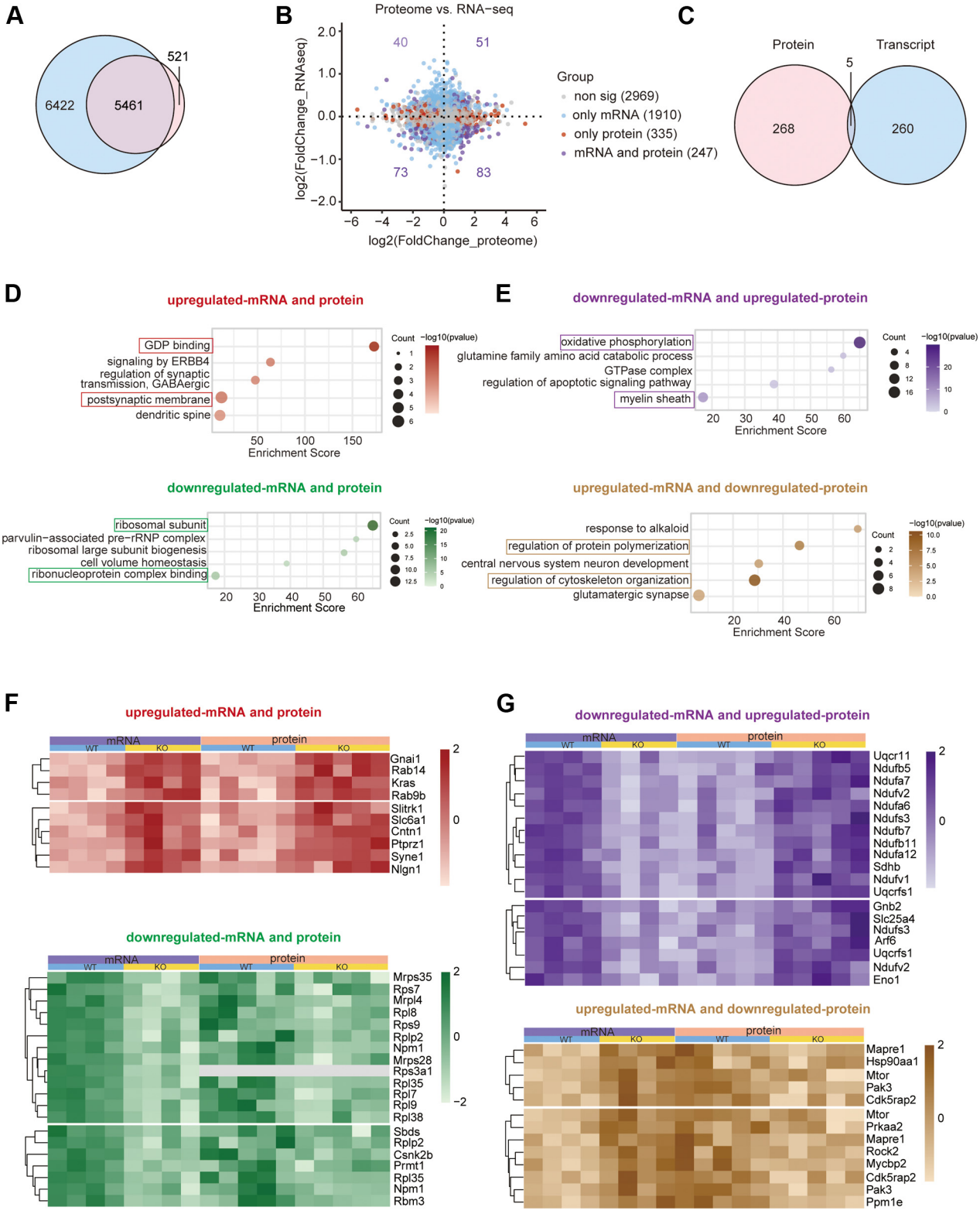

FIG. 4. **Proteomic and transcriptomic correlation analysis in S1 cortex of the *Nsun5*-KO and WT mice.** *A*, venn diagrams comparing the overlap of expressed transcripts and proteins between *Nsun5*-KO and WT mice, highlighting unique and shared entities. *B*, scatter plot displaying the relationship between changes in transcriptome and proteome profiles, with log2 fold change of proteins on the *x*-axis and log2 fold change of genes on the *y*-axis. Color coding indicates significance and type of expression: *blue* for mRNA only, *red* for proteins only, and *purple*

and motor cortices. Notably, the S1 cortex is essential for sensory perception, including the discrimination of tactile features such as shape, size, and texture (39). Given Nsun5's cortical expression pattern and the pronounced morphological changes observed, we employed multi-omics approaches to investigate the molecular alterations in the S1 cortex following Nsun5 deficiency. Multi-omics analyses indicated alterations in the expression of various genes and proteins, which were implicated in the regulation of translation, cellular metabolism, and neurotransmission, underscoring the critical and diverse roles of Nsun5 in the brain.

Our targeted metabolomics analyses revealed significant decreases in multiple neurotransmitters in *Nsun5*-KO mice. Neurotransmitters—such as acetylcholine, glycine, (5-HIAA, and octopamine—are directly involved in neuronal signaling and thus influence emotion, cognition, motor control, and pain perception (40). Moreover, polyamines (*e.g.*, putrescine) and cysteine provide cell repair and antioxidant protection, supporting neural cell regeneration under oxidative stress (41). These findings suggest that Nsun5 deficiency leads to aberrant neurotransmitter homeostasis, which may underlie the observed abnormalities in motor, emotional, cognitive, and pain-related functions. Focusing on the pain-related aspects, our transcriptomic and proteomic analyses identified multiple differentially expressed molecules—such as decarboxylase, Plk1, Sst, and Rtn4r—known to be involved in pain regulation. GO enrichment further confirmed that the dysregulated molecular landscapes in both transcriptomes and proteomes encompass biological processes directly associated with pain modulation, including the regulation of membrane potential, voltage-gated channel activity, neuron-to-neuron synapse function, and neurotransmitter transport. Together, these findings highlight a mechanistic link between Nsun5 deficiency, altered neurotransmitter levels, and the molecular pathways underlying pain perception. We further focused on the changes in pain-related molecules and confirmed through behavioral assays that the deletion of Nsun5 reduced pain sensitivity. This study not only reveals the novel function of Nsun5 in regulating S1 cortex thickness and pain perception but also lays the groundwork for exploring its potential roles in other brain regions and its broader impact on neural health.

Evidences indicated that NSUN5 methylated C3782 of human and C3438 of mouse 28S ribosomal RNA (2, 42). Besides, lacking C^5-methylation at 25S rRNA residue C2278 in yeast altered ribosomal structure and translational fidelity (43). Ding *et al*. investigated Nsun5 in the regulation of mRNA decay and stability by m^5C modification (44), but how NSUN5 affect the translation of different genes is still unclear. We performed comprehensive transcriptomic and proteomic profiling to characterize the downstream effects of Nsun5 deficiency. In *Nsun5*-KO mice, we observed widespread dysregulation at both the transcript and protein levels. Molecules exhibiting parallel changes in mRNA and protein abundance clustered into distinct functions. Those consistently downregulated were mainly involved in core cellular processes—such as ribosomal assembly, protein synthesis precursors, and ribonucleoprotein processing—while those consistently upregulated were associated with synaptic activity, neuronal signaling, and postsynaptic architecture. A subset of molecules, however, displayed discordant trends between transcript and protein expression. Genes with reduced mRNA but increased protein abundance were enriched in pathways related to energy metabolism, GTPase activity, apoptotic regulation, and myelin formation, suggesting posttranslational or proteolytic control. Conversely, genes with elevated mRNA but lower protein levels were linked to protein polymerization, neuron development, cytoskeletal organization, and synapses. Taken together, these findings highlight loss of Nsun5 disrupts the normal balance of translation and processing. Although we did not further dissect these intricate regulatory cascades, our data suggest that Nsun5 likely participates in additional, as yet uncharacterized functions critical for neural development and physiology.

In summary, we employed a comprehensive multi-omics approach to reveal the regulatory effects of Nsun5 on transcripts, proteins, and neurotransmitters in the S1 cortex and discovered a novel phenotype in which Nsun5 knockout impaired pain sensation. Our data also provide insights into Nsun5's crucial role in the nervous system through its impact on the regulation of translation, cellular metabolism, and neurotransmission.

DATA AVAILABILITY

The DIA MS raw data and spectral libraries generated during this study were available in the ProteomeXchange Consortium *via* the iProX partner repository with the dataset identifier PXD053689. The data set PXD053689 has access rights of Public. The access link for the data on ProteomeXchange is: http://proteomecentral.proteomexchange.org/cgi/GetDataset?ID=PXD053689. The access link for the data on iProX is: https://www.iprox.cn/page/project.html?id=IPX0009183000.

Supplemental data—This article contained supplemental data.

Acknowledgments—We are grateful to Dr B. Shen for providing *Nsun5*-KO mice. This work was supported by STI2030-Major Projects (2022ZD0211600), the National

for both. *C*, venn diagrams detailing the numbers of differentially expressed transcripts and proteins, showing distinct and overlapping changes in *Nsun5*-KO compared to WT. *D* and *E*, GO analysis of differentially expressed molecules in the transcriptome and proteome, with functional enrichments plotted. *F* and *G*, the heatmap displays the expression of differentially expressed molecules within the selected GO terms (*solid-line boxes*) under conditions where mRNA and protein expression are either consistent or inconsistent. GO, Gene Ontology.

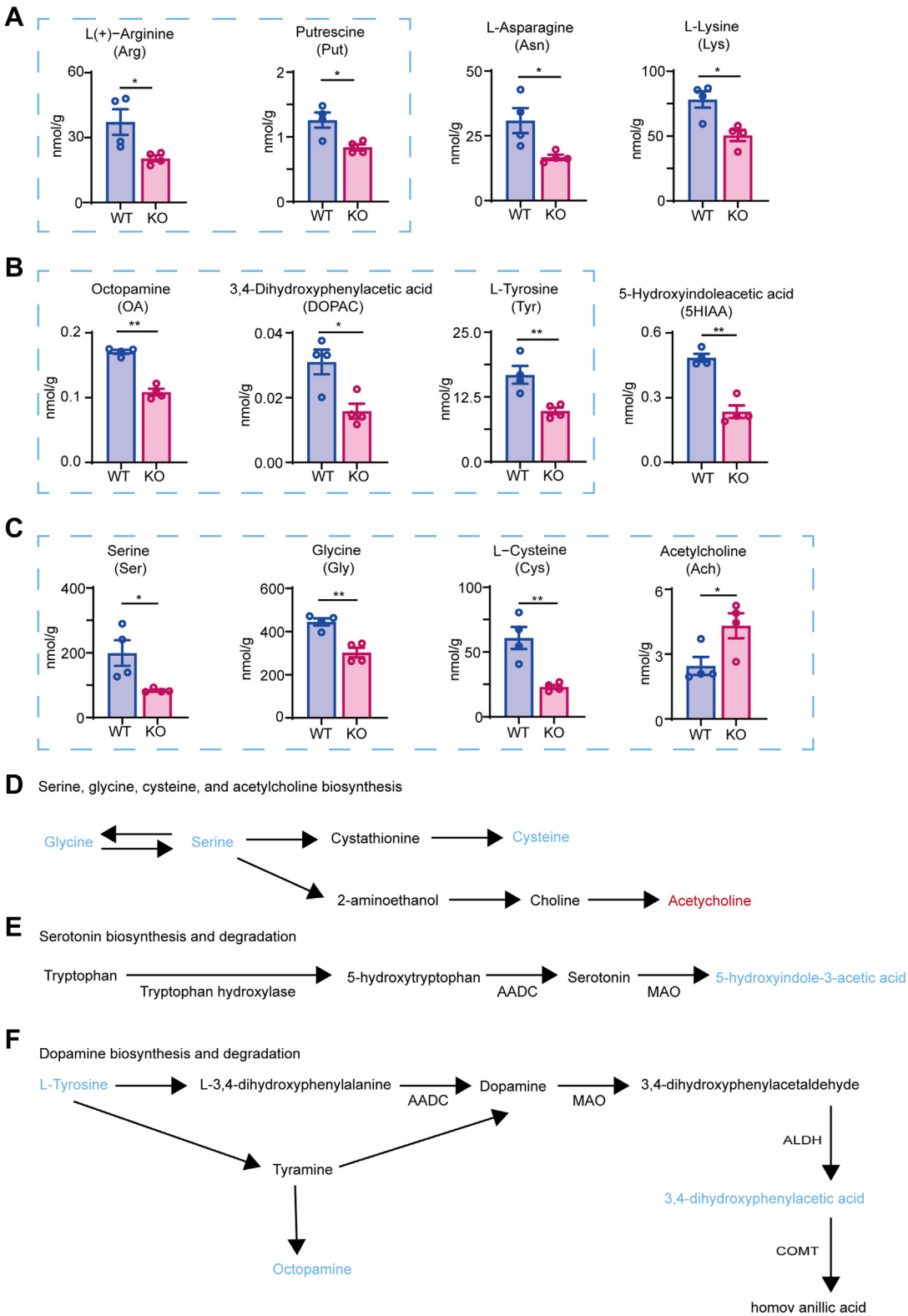

FIG. 5. **Alterations in neurotransmitters and metabolites in the S1 cortex of *Nsun5*-KO *versus* WT mice.** *A–C*, bar graphs showing significant differences in the levels of various neurotransmitters and their metabolites between WT and *Nsun5*-KO mice, with decreases noted in several compounds. N = 4 biological replicates for WT and KO group, respectively. Two-tailed independent *t* test. Error bars represent ±SEM, with $^{*}p < 0.05$ and $^{**}p < 0.01$ indicating levels of statistical significance. *D–F*, schematic diagrams illustrating the biosynthetic pathways for serine, glycine, cysteine, acetylcholine, serotonin, and dopamine, highlighting potential metabolic disruptions in *Nsun5*-KO mice.

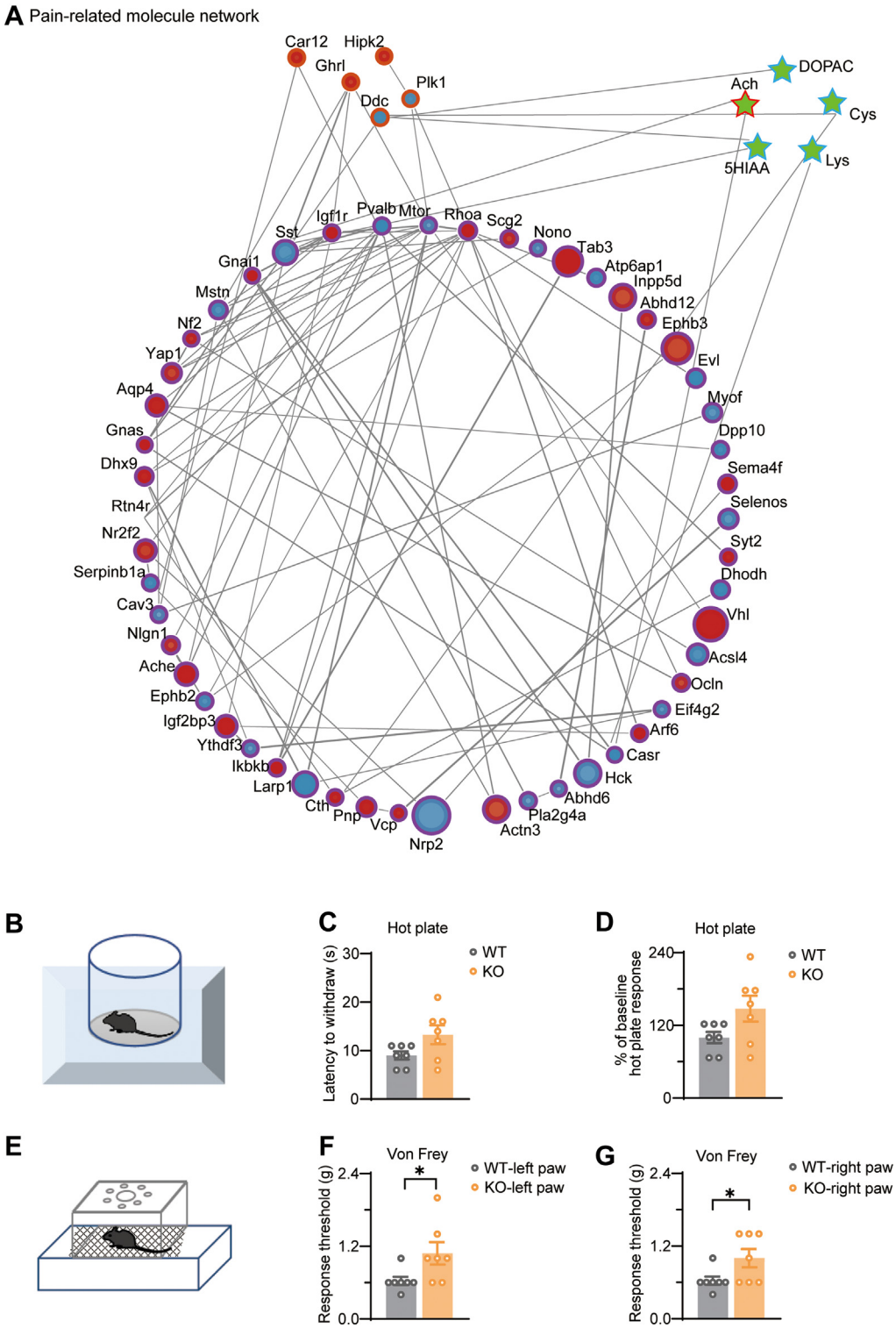

FIG. 6. **Impairment of pain sensation in *Nsun5*-KO mice.** *A*, network diagram depicting the interactions among transcripts, proteins, and neurotransmitters associated with pain sensation, constructed using String and Cytoscape software. Nodes represent molecules, and edges indicate known interactions. *B* and *E*, illustrations of the experimental setups used to measure pain response: (*B*) hot plate test, and (*E*) Von Frey filament test for mechanical pain sensitivity. *C* and *D*, hot plate test results showing the latency to respond to heat in seconds (*C*) and the percentage of baseline pain response (*D*) for *Nsun5*-KO mice *versus* WT littermates. *F* and *G*, Von Frey test results measuring the mechanical pain threshold for the *left* (*F*) and *right* (*G*) paws in *Nsun5*-KO mice compared to WT. N = 7 biological replicates for WT and KO group, respectively. Two-tailed independent *t* test. Error bars represent ±SEM, with $^{*}p < 0.05$ and $^{**}p < 0.01$ denoting statistical significance.

Natural Science Foundation of China (82272174 and 81827901), the Science and Technology Innovation Action Plan of STCSM (22S31901900), and the innovative research team of the high-level local university in Shanghai, as well as by the NHC Key Laboratory of Glycoconjugates Research.

Author contributions—P. C., H. Z., and X. G. data curation; P. C., H. Z., and J. X. formal analysis; P. C., Z. H., and H. S. methodology; P. C., and H. S. writing–original draft; P. C. and H. S. investigation; Z. H. and H. S. project administration; Z. H. and H. S. conceptualization; Z. H. and H. S. writing–review and editing; H. S. supervision; H. S. funding acquisition.

Conflict of interest—The authors declare no competing interests.

Abbreviations—The abbreviations used are: ACh, acetylcholine; Ache, acetylcholinesterase; ACN, acetonitrile; cDNA, complementary DNA; DA, dopamine; DOPAC, 3, 4-dihydroxyphenylacetic acid; FA, formic acid; FDR, false discovery rate; GO, Gene Ontology; 5-HIAA, 5-hydroxyindoleacetic acid; KEGG, Kyoto Encyclopedia of Genes and Genomes; RT-PCR, real-time quantitative PCR; Xdh, xanthine dehydrogenase/oxidase.

Received July 6, 2024, and in revised form, February 27, 2025
Published, MCPRO Papers in Press, April 1, 2025, https://doi.org/10.1016/j.mcpro.2025.100960

REFERENCES

1. Boccaletto, P., Machnicka, M. A., Purta, E., Piatkowski, P., and Bujnicki, J. M. (2018) MODOMICS: a database of RNA modification pathways. 2017 update. *Nucleic Acids Res.* **46**, D303–D307
2. Heissenberger, C., Liendl, L., Nagelreiter, F., Gonskikh, Y., and Schosserer, M. (2019) Loss of the ribosomal RNA methyltransferase NSUN5 impairs global protein synthesis and normal growth. *Nucleic Acids Res.* **47**, 11807–11825
3. Janin, M., Ortiz-Barahona, V., de Moura, M. C., Martinez-Cardus, A., and Esteller, M. (2019) Epigenetic loss of RNA-methyltransferase NSUN5 in glioma targets ribosomes to drive a stress adaptive translational program. *Acta Neuropathol.* **138**, 1053–1074
4. Wang, Y., Jiang, T., Xu, J., Gu, Y., and Hu, Z. (2021) Mutations in RNA methyltransferase gene NSUN5 confer high risk of outflow tract malformation. *Front. Cell Dev. Biol.* **9**, 623394
5. Xue, M., Shi, Q., Zheng, L., Li, Q., Yang, L., and Zhang, Y. (2020) Gene signatures of m5C regulators may predict prognoses of patients with head and neck squamous cell carcinoma. *Am. J. Transl. Res.* **12**, 6841–6852
6. Zhang, X. W., Wu, L. Y., Liu, H. R., Huang, Y., and Wu, H. G. (2022) NSUN5 promotes progression and predicts poor prognosis in hepatocellular carcinoma. *Oncol. Lett.* **24**, 439
7. Chen, P., Zhang, T., Yuan, Z., Shen, B., and Chen, L. (2019) Expression of the RNA methyltransferase Nsun5 is essential for developing cerebral cortex. *Mol. Brain* **12**, 74
8. Zhang, T., Chen, P., Li, W., Sha, S., and Chen, L. (2019) Cognitive deficits in mice lacking Nsun5, a cytosine-5 RNA methyltransferase, with impairment of oligodendrocyte precursor cells. *Glia* **67**, 688–702
9. Yuan, Z., Chen, P., Zhang, T., Shen, B., and Chen, L. (2019) Agenesis and hypomyelination of corpus callosum in mice lacking Nsun5, an RNA methyltransferase. *Cells* **8**, 552
10. Eickhoff, S. B., Jbabdi, S., Caspers, S., Laird, A. R., Fox, P. T., Zilles, K., *et al*. (2010) Anatomical and functional connectivity of cytoarchitectonic areas within the human parietal operculum. *J. Neurosci.* **30**, 6409–6421
11. Eimer, M., and Katus, T. (2020) Shifts of spatial attention in visual and tactile working memory are controlled by independent modality-specific mechanisms. *Cereb. Cortex* **30**, 296–310
12. Lee, S., Kruglikov, I., Huang, Z. J., Fishell, G., and Rudy, B. (2013) A disinhibitory circuit mediates motor integration in the somatosensory cortex. *Nat. Neurosci.* **16**, 1662–1670
13. Zhu, X., Tang, H. D., Dong, W. Y., Kang, F., and Zhang, Z. (2021) Distinct thalamocortical circuits underlie allodynia induced by tissue injury and by depression-like states. *Nat. Neurosci.* **24**, 542–553
14. Prescott, S. A., Ma, Q., and De Koninck, Y. (2014) Normal and abnormal coding of somatosensory stimuli causing pain. *Nat. Neurosci.* **17**, 183–191
15. Wimmer, V. C., Bruno, R. M., de Kock, C. P., Kuner, T., and Sakmann, B. (2010) Dimensions of a projection column and architecture of VPM and POm axons in rat vibrissal cortex. *Cereb. Cortex* **20**, 2265–2276
16. Canavero, S., and Bonicalzi, V. (2013) Role of primary somatosensory cortex in the coding of pain. *Pain* **154**, 1156–1158
17. Niu, Y., Shen, B., Cui, Y., Chen, Y., and Sha, J. (2014) Generation of gene-modified cynomolgus monkey *via* cas9/RNA-mediated gene targeting in one-cell embryos. *Cell* **156**, 836–843
18. Abraham, A. D., Leung, E. J. Y., Wong, B. A., Rivera, Z. M. G., Kruse, L. C., Clark, J. J., *et al*. (2020) Orally consumed cannabinoids provide long-lasting relief of allodynia in a mouse model of chronic neuropathic pain. *Neuropsychopharmacology* **45**, 1105–1114
19. Katzman, A., Khodadadi-Jamayran, A., Kapeller-Libermann, D., Ye, X., Tsirigos, A., Heguy, A., *et al*. (2021) Distinct transcriptomic profiles in the dorsal Hippocampus and prelimbic cortex are transiently regulated following episodic learning. *J. Neurosci.* **41**, 2601–2614
20. Wang, J., Xu, S. L., Duan, J. J., Yi, L., and Yu, S. C. (2019) Invasion of white matter tracts by glioma stem cells is regulated by a NOTCH1-SOX2 positive-feedback loop. *Nat. Neurosci.* **22**, 91–105
21. Perreau-Lenz, S., Sanchis-Segura, C., Leonardi-Essmann, F., Schneider, M., and Spanagel, R. (2010) Development of morphine-induced tolerance and withdrawal: involvement of the clock gene mPer2. *Eur. Neuropsychopharmacol.* **20**, 509–517
22. Cheng, L. C., Murugaiyah, V., and Chan, K. L. (2015) Flavonoids and phenylethanoid glycosides from Lippia nodiflora as promising anti-hyperuricemic agents and elucidation of their mechanism of action. *J. Ethnopharmacol.* **176**, 485–493
23. Khoury, S., Piltonen, M. H., Ton, A. T., Cole, T., and Diatchenko, L. (2019) A functional substitution in the L-aromatic amino acid decarboxylase enzyme worsens somatic symptoms *via* a serotonergic pathway. *Ann. Neurol.* **86**, 168–180
24. Zhang, J., Zhao, H., Zhang, A., Zhao, C., and Liang, D. (2022) Identifying a novel KLF2/lncRNA SNHG12/miR-494-3p/RAD23B axis in Spare Nerve Injury-induced neuropathic pain. *Cell Death Discov.* **8**, 272
25. Deng, X., Wang, D., Wang, S., Wang, H., and Zhou, H. (2018) Identification of key genes and pathways involved in response to pain in goat and sheep by transcriptome sequencing. *Biol. Res.* **51**, 25
26. Tiwari, V., Yang, F., He, S. Q., Shechter, R., and Raja, S. N. (2016) Activation of peripheral mu-opioid receptors by dermorphin [D-Arg2, Lys4] (1-4) amide leads to modality-preferred inhibition of neuropathic pain. *Anesthesiology* **124**, 706–720
27. Dimidschstein, J., Passante, L., Dufour, A., van den Ameele, J., and Vanderhaeghen, P. (2013) Ephrin-B1 controls the columnar distribution of cortical pyramidal neurons by restricting their tangential migration. *Neuron* **79**, 1123–1135
28. Jakob, B., Kochlamazashvili, G., Japel, M., Gauhar, A., Bock, H. H., Maritzen, T., *et al*. (2017) Intersectin 1 is a component of the Reelin pathway to regulate neuronal migration and synaptic plasticity in the hippocampus. *Proc. Natl. Acad. Sci. U. S. A.* **114**, 5533–5538
29. Yoon, I. S., Li, P. P., Siu, K. P., Kennedy, J. L., Cooke, R. G., Parikh, S. V., *et al*. (2001) Altered IMPA2 gene expression and calcium homeostasis in bipolar disorder. *Mol. Psychiatry* **6**, 678–683
30. Trimouille, A., Marguet, F., Sauvestre, F., Lasseaux, E., and Laquerriere, A. (2020) Foetal onset of EIF2B related disorder in two siblings: cerebellar hypoplasia with absent Bergmann glia and severe hypomyelination. *Acta Neuropathol. Commun.* **8**, 48
31. Yamamoto, K., Ruuskanen, J. O., Wullimann, M. F., and Vernier, P. (2010) Two tyrosine hydroxylase genes in vertebrates New dopaminergic territories revealed in the zebrafish brain. *Mol. Cell Neurosci.* **43**, 394–402

32. Meiser, J., Weindl, D., and Hiller, K. (2013) Complexity of dopamine metabolism. *Cell Commun. Signal.* **11**, 34
33. Pourhamzeh, M., Moravej, F. G., Arabi, M., Shahriari, E., and Joghataei, M. T. (2022) The roles of serotonin in neuropsychiatric disorders. *Cell Mol. Neurobiol.* **42**, 1671–1692
34. Guan, Z., Kuhn, J. A., Wang, X., Colquitt, B., and Basbaum, A. I. (2016) Injured sensory neuron-derived CSF1 induces microglial proliferation and DAP12-dependent pain. *Nat. Neurosci.* **19**, 94–101
35. Liu, H., Su, D., Liu, L., Chen, L., and Wang, J. (2020) Identification of a new functional domain of Nogo-A that promotes inflammatory pain and inhibits neurite growth through binding to NgR1. *FASEB J.* **34**, 10948–10965
36. Dhanasobhon, D., Medrano, M. C., Becker, L. J., Moreno-Lopez, Y., and Cordero-Erausquin, M. (2021) Enhanced analgesic cholinergic tone in the spinal cord in a mouse model of neuropathic pain. *Neurobiol. Dis.* **155**, 105363
37. Bannon, A. W., and Malmberg, A. B. (2007) Models of nociception: hot-plate, tail-flick, and formalin tests in rodents. *Curr. Protoc. Neurosci.* Chapter 8 https://doi.org/10.1002/0471142301.ns0809s41
38. Toussaint, A. B., Foster, W., Jones, J. M., Kaufmann, S., and Abdus-Saboor, I. (2022) Chronic paternal morphine exposure increases sensitivity to morphine-derived pain relief in male progeny. *Sci. Adv.* **8**, eabk2425
39. Tamè, L., and Longo, M. R. (2023) Emerging principles in functional representations of touch. *Nat. Rev. Psychol.* **2**, 459–471
40. Sheffler, Z. M., Reddy, V., and Pillarisetty, L. S. (2024) *Physiology, Neurotransmitters*. StatPearls, Treasure Island (FL)
41. Xuan, M., Gu, X., Li, J., Huang, D., Xue, C., and He, Y. (2023) Polyamines: their significance for maintaining health and contributing to diseases. *Cell Commun. Signal.* **21**, 348
42. Sharma, S., Yang, J., Watzinger, P., Kotter, P., and Entian, K. D. (2013) Yeast Nop2 and Rcm1 methylate C2870 and C2278 of the 25S rRNA, respectively. *Nucleic Acids Res.* **41**, 9062–9076
43. Schosserer, M., Minois, N., Angerer, T. B., Amring, M., and Grillari, J. (2015) Methylation of ribosomal RNA by NSUN5 is a conserved mechanism modulating organismal lifespan. *Nat. Commun.* **6**, 6158
44. Ding, C., Lu, J., Li, J., Hu, X., and Huang, B. (2022) RNA-methyltransferase Nsun5 controls the maternal-to-zygotic transition by regulating maternal mRNA stability. *Clin. Transl. Med.* **12**, e1137